Research article

Unleashing the electrochemical performance of zirconia nanoparticles on valve-regulated lead acid battery

Sanjay H. Rajur [a], Bipin S. Chikkatti [b], Abdulwasa Bakr Barnawi [c], Javed Khan Bhutto [c], T. M. Yunus Khan [d], Ashok M. Sajjan [b,e,*], Nagaraj R. Banapurmath [e], A.B. Raju [a]

[a] *Department of Electrical and Electronics Engineering, KLE Technological University, Hubballi, 580031, India*
[b] *Department of Chemistry, KLE Technological University, Hubballi, 580031, India*
[c] *Department of Electrical Engineering, College of Engineering, King Khalid University, Abha, 61421, Saudi Arabia*
[d] *Department of Mechanical Engineering, College of Engineering, King Khalid University, Abha, 61421, Saudi Arabia*
[e] *Centre of Excellence in Material Science, School of Mechanical Engineering, KLE Technological University, Hubballi, 580031, India*

A R T I C L E   I N F O

A B S T R A C T

The electrochemical act of valve-regulated lead acid batteries can be enhanced by conductive materials like metal oxides. This work aims to examine the preparation and influence of zirconia on poly(vinyl alcohol) based gel valve-regulated lead acid battery. Characterizations like Fourier transform infrared spectroscopy, ionic conductivity, water retention study, cyclic voltammetry, electrochemical impedance spectroscopy and galvanostatic charge-discharge techniques were done. The optimized gel system exhibited a discharge capacity of 198.45 μAh cm^{-2} at the current density of 0.6 mA cm^{-2}. The battery cell with an optimized gel matrix displayed a maximum discharge capacity of 22.5 μAh at a current of 20 μA. After 500 continuous cycles, the battery attained a discharge capacity retention of 91 %. The presence of zirconia will increase the electrochemical performance of gel valve-regulated lead acid batteries.

1. Introduction

Energy consumption has been on the rise globally during the last few decades. In the past, fossil fuels were mostly used to generate electricity [1]. Energy consumption rises as a result of population increase, industrialization, and economic expansion, especially in developing nations with large populations. Growing demand creates environmental difficulties with climate change and global warming, air pollution's effects on human health, and the possibility of terrestrial and aquatic life [2]. Chemical energy is the most suitable type of storage for energy with regard to energy density. Batteries offer chemical energy that can be delivered as electricity with a high conversion rate and no gaseous emission for this purpose. Therefore, affordable, secure, rechargeable batteries with sufficient voltage and rate capabilities are of major importance [3]. The highest market share for rechargeable batteries in terms of sales value and production MWh belongs to lead-acid batteries, which are provided by a significant, well-established global supplier base. The bulk of industrial batteries are used in standby applications to deliver safe power for national security, data networks, telecommunications, and many more applications where the continuity of the electrical supply is crucial [4]. The primary energy

---

* Corresponding author. Department of Chemistry, KLE Technological University, Hubballi, 580031, India.
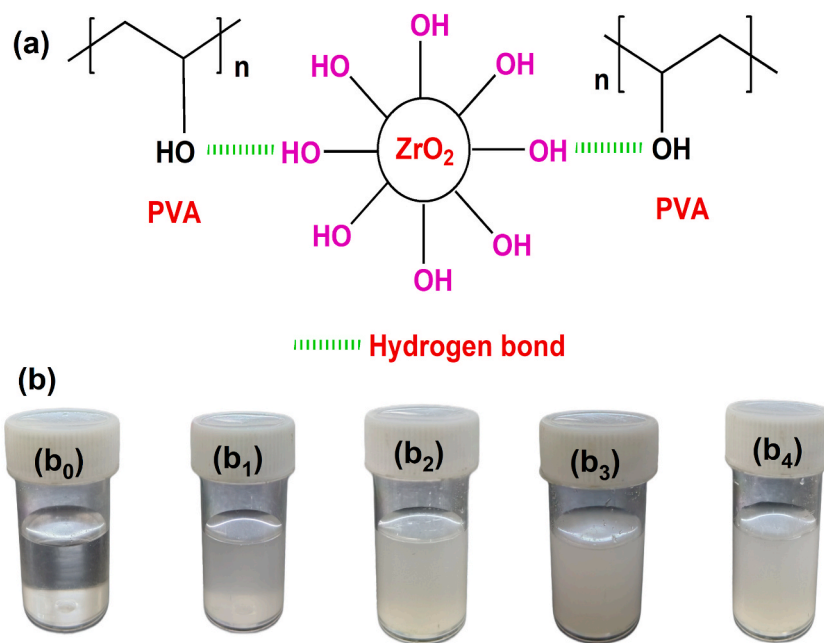*E-mail address:* am_sajjan@kletech.ac.in (A.M. Sajjan).

Fig. 1. (a) Reaction between ZrO_2 nanoparticles and PVA (b) Photo images of plane PVA (b_0), 0.5 wt% ZrO_2@PVA (b_1), 1 wt% ZrO_2@PVA (b_2), 1.5 wt% ZrO_2@PVA (b_3) and 2 wt% ZrO_2@PVA (b_4).

storage component of modern Indian telecommunications power supply units is the valve-regulated lead acid (VRLA) battery. VRLA batteries are categorized into two categories based on how they immobilize the electrolyte: GEL and AGM batteries are two types of batteries [5]. A gel thickening agent is used in the GEL battery to spread the electrolyte evenly throughout the cell plates and separators while preventing it from flowing. In an AGM battery, the plates are kept apart and in touch with the electrolyte by a highly porous and absorbent glass fibre mat. Recombinant batteries include GEL and AGM batteries. This implies that the negative plates of all lead acid batteries absorb the oxygen that is typically created on the positive plates [6].

A well-known water-soluble, semicrystalline, and biodegradable synthetic polymer called poly(vinyl alcohol) (PVA) is formed by hydrolyzing poly(vinyl acetate) [7]. PVA has a wide range of intriguing physiochemical properties. PVA, to mention a few, offers outstanding film-forming abilities, biocompatibility, optical characteristics, adhesive qualities, and emulsifying properties [8–10]. PVA contains an interchain hydrogen bond because of the hydroxyl groups that are present. PVA's high melting point and strong mechanical stability are a result of this [11]. PVA attracted great interest in the fields of drug delivery [12], fuel cells [13], sensors [14], wound dressing [15] and supercapacitors [16]. Due to the formation of potent hydrogen bonds between PVA's hydroxyl groups and the hydrophilic surfaces of the nanofillers, PVA is very attractive as a matrix for nanofillers [17]. Zhu et al., in 2012 presented that PVA can be utilized as an electrolyte for lithium-ion batteries [18].

According to reports, the dispersion of nanofillers like SiO_2, Al_2O_3, TiO_2, ZrO_2, etc., in polymers can operate as solid plasticizers to stop the polymer chains from crystallizing or reorganizing and to improve ionic mobility and ionic dissociation [19]. ZrO_2 has been a popular addition among them due to its high hydrophilicity and chemical stability in both acidic and alkaline environments [20]. Zirconia (ZrO_2) is an inorganic transition metal oxide with a high concentration of surface oxygen defects, acidic surface-active sites, robust thermal and chemical stability, and a great ion exchange capacity [21]. The incorporation of nanopowder fillers within the polymer substrate introduced imperfections and greater void spaces at the interface between the fillers and the polymer chain. This phenomenon elucidates the observed elevation in ionic conductivity within the nanofiller polymer gel electrolyte. Utilizing ZrO_2 particles as a solid plasticizer in polymer electrolytes offers improved electrochemical properties, owing to its recognized chemical inertness and stability under acidic conditions [22]. Jiang et al. reported that ZrO_2 can increase the performance of the vanadium redox flow battery [23]. Because ZrO_2 possesses several desirable physicochemical properties that are crucial for technology, it is frequently employed in a variety of applications like biomedical implants [24], sensors [25], fuel cells [26], composite coatings [27], and lithium-ion batteries [28]. Mansuroglu et al. reported that 0.6 wt% S-GrOP showed better electrochemical properties [29]. Gencten et al. reported that the combination of 6 wt% fumed silica and 3 wt% of TiO_2 displayed better electrochemical performances [30].

The PVA gel electrolyte functions similarly to liquid acid to enable the electrochemical reactions that produce electricity in the battery. The additive ZrO_2 will enhance the electrochemical performance of the battery. The motto of this study is to prepare of PVA-based gel polymer electrolyte comprising ZrO_2 and analyze its physiochemical and electrochemical properties for gel-VRLA batteries. To our knowledge, no one has reported the use of the ZrO_2@PVA gel matrix for VRLA batteries.
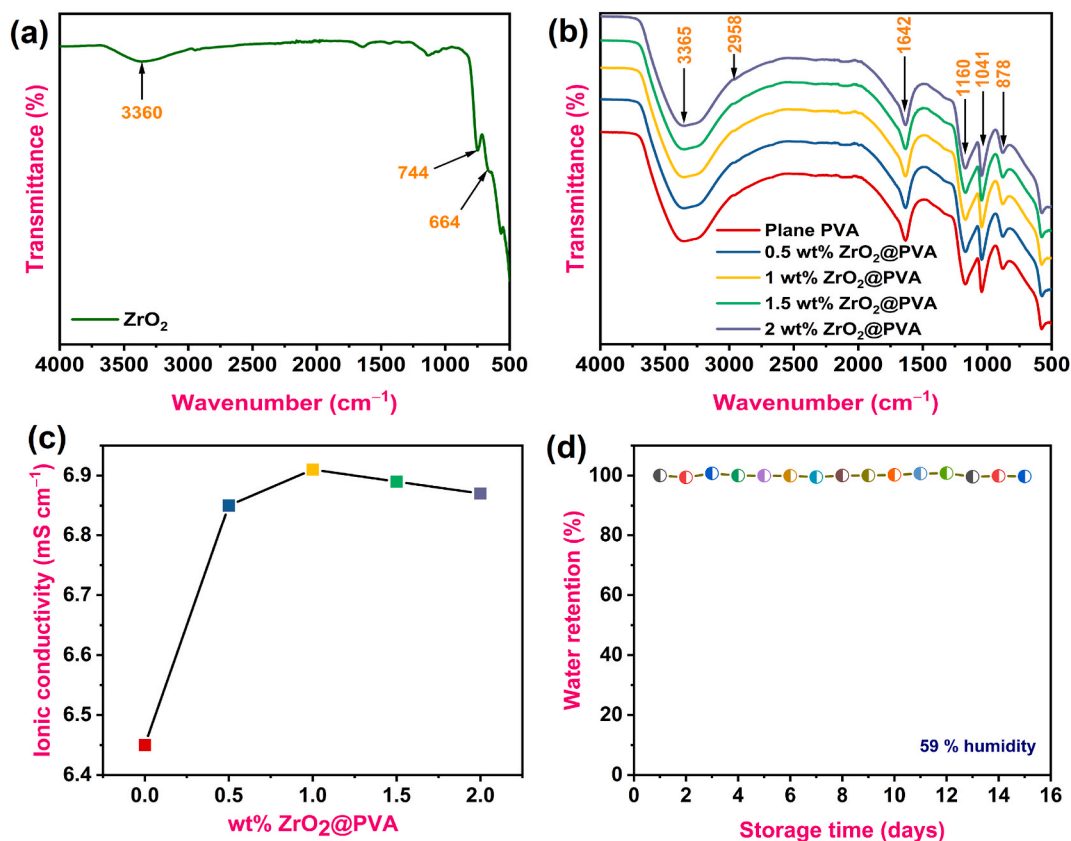
Fig. 2. (a) FTIR of ZrO_2 nanoparticles (b) FTIR of plane PVA and different ZrO_2 incorporated PVA gels (c) Variation ionic conductivity of formulated gels (d) Water retention study of 1 wt% ZrO_2@PVA

2. Experiments

2.1. Chemicals

Poly(vinyl alcohol) with a molecular weight of approximately 124,000 was obtained from S.D. Fine Chemicals Ltd. in Mumbai, India. Zirconia nanoparticles with a size of ≤100 nm were purchased from Sigma Aldrich Company in the USA. Sulphuric acid was supplied by Spectrum Reagent and Chemicals Pvt. Ltd. in Cochin, India.

2.2. Synthesis of gel systems

8 wt% of PVA was dissolved in 36 wt% H_2SO_4 at 60 °C with a constant stirring for about 3 h. The attained gel matrix is designated as plane PVA. To develop ZrO_2 nanoparticles combined PVA gel matrix, a known quantity of ZrO_2 was dissolved in a PVA gel electrolyte at room temperature with a constant stirring for about 24 h. The quantity of ZrO_2 varied as 0.5 %, 1 %, 1.5 %, and 2 wt% to PVA, and gel electrolytes thus developed were designated as 0.5 wt% ZrO_2@PVA, 1 wt% ZrO_2@PVA, 1.5 wt% ZrO_2@PVA and 2 wt% ZrO_2@PVA, respectively. Fig. 1(a) and (b) designate hydrogen-bonded interaction between ZrO_2 and PVA and photo images of formulated gel electrolytes, respectively.

2.3. Study of gel matrix

The gel systems underwent analysis using FTIR (Fourier Transform Infrared Spectroscopy) with equipment from PerkinElmer Pvt. Ltd in Singapore to explore the reaction dynamics between ZrO_2 and PVA within the gel matrix. Subsequently, the ionic conductivity of the gels was measured using EQ-662 conductivity meter manufactured by Equip-Tronics in Mumbai, India. Water retention of the gel structure was analyzed for continuous 15 days. Cyclic voltammetry (CV), electrochemical impedance spectroscopy (EIS), and galvanostatic charge-discharge (GCD) practices were employed to investigate the electrochemical characteristics of the gel matrix. CV graphs were generated across various scan rates spanning from 10 to 150 mV s^{-1}, maintaining a potential range of −1 to +1 V. EIS assessments were conducted at the respective open circuit potentials (OCPs) over a frequency range of 1 Hz–100 kHz, employing a 5 mV amplitude. These comprehensive analyses provided detailed insights into the electrochemical behavior and properties of the gel
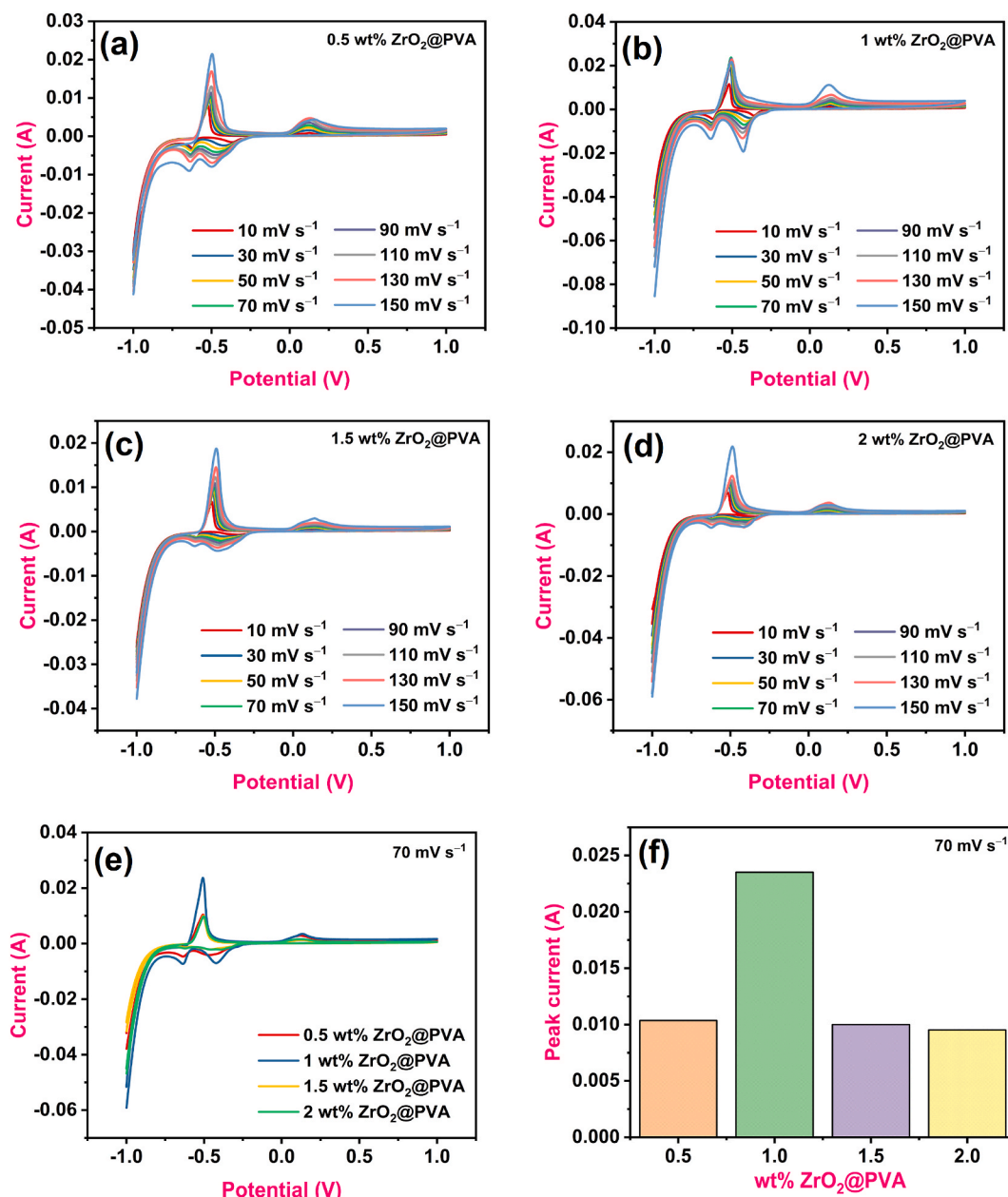
Fig. 3. (a–d) Cyclic voltammogram of 0.5 wt% ZrO$_2$@PVA, 1 wt% ZrO$_2$@PVA, 1.5 wt% ZrO$_2$@PVA and 2 wt% ZrO$_2$@PVA, respectively (e) CV graphs of all gel systems at 70 mV s^{-1} (f) Discrepancy of peak current concerning different wt% of ZrO$_2$ in PVA at 70 mV s^{-1}

systems, offering valuable information for their potential applications and performance optimization. To evaluate the performance of a prototype battery, a specialized cell was constructed featuring two negative electrodes and two positive electrodes, each with dimensions of 2×2 cm^2. This cell was optimized with a gel system totaling 4.5 ml in volume. GCD tests were directed at various current densities, alongside cycle studies, to assess its functionality. For electrochemical analysis, a CHI660E electrochemical workstation from CH Instruments in Texas, USA, was utilized. The system employed a 3-electrode configuration for CV and EIS, consisting of lead as the working electrode, platinum wire as the counter electrode, and Ag/AgCl, (saturated) KCl as the reference electrode. The lead rod underwent polishing before testing, and precautions were taken to prevent contact with the electrodes during testing. In GCD testing, a 2-electrode system was employed, providing further insight into the battery's discharge behavior under different conditions.
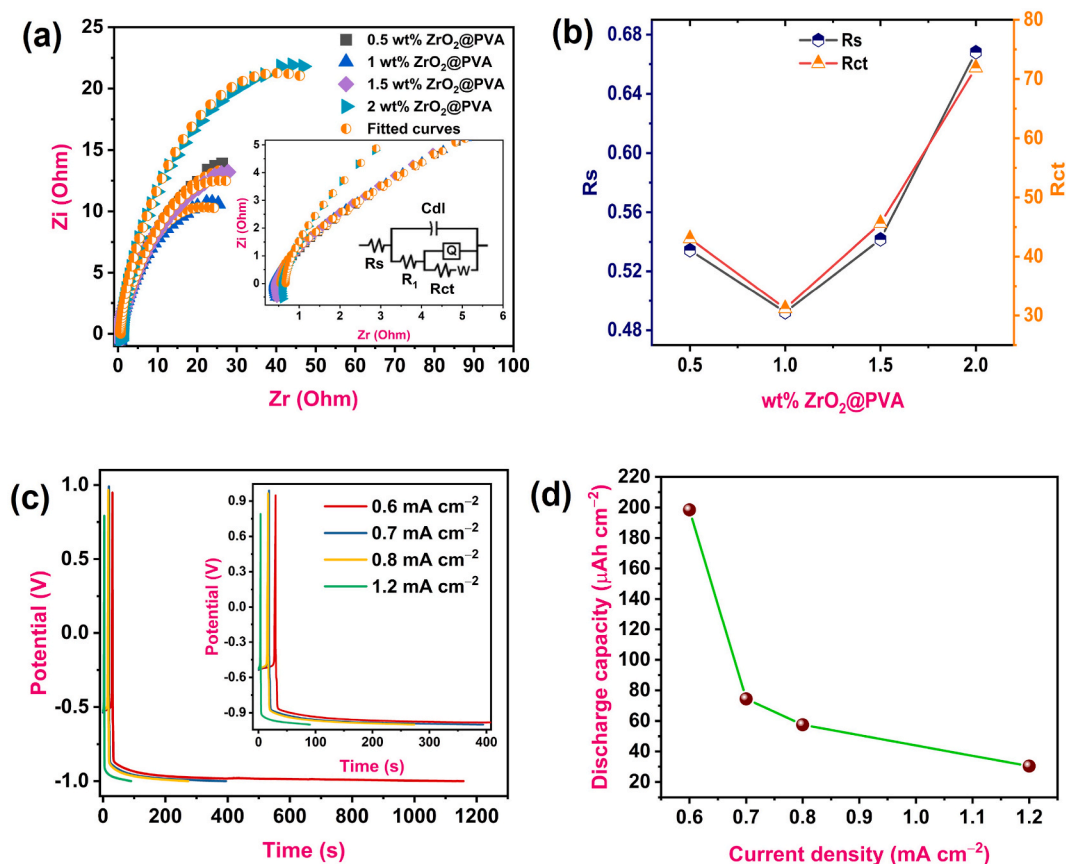
Fig. 4. (a) Nyquist plot of gel systems (b) Rs and Rct of gel systems (c) Galvanostatic charge-discharge curves of 1 wt% ZrO$_2$@PVA gel at different current densities (d) Variation of discharge capacity concerning different current densities.

3. Results and discussions

3.1. FTIR analysis

FTIR spectrum of plane ZrO$_2$ nanoparticles is displayed in Fig. 2(a). A large peak at around 3360 cm^{-1} indicates the presence of a stretching vibration of hydroxyl group molecules on the exterior of ZrO$_2$ powder [31]. The existence of Zr–O metal-oxygen bonding is shown by the strong and powerful stretching vibration band at 744 and 664 cm^{-1} [32]. Fig. 2(b) illustrates FTIR spectra of plane PVA and ZrO$_2$-incorporated PVA gels. The key peaks of PVA were observed at 3365, 2958 and 1642 cm^{-1}. These peaks are allotted to the O–H stretching vibration of the hydroxy group, CH$_2$ asymmetric stretching vibration, and C=O carbonyl stretch, respectively [33–35]. The bands at 1160 and 1041 cm^{-1} are designated for C–O stretching of acetyl groups [36]. It is possible to conclude that there was no alteration to the wavelength's location or shape with respect to the PVA matrix. This behavior indicates that the approach cannot identify the possibility of a physical connection between the polymeric matrix and the nanoparticles or the chemical interaction between the phases that occurs through low-intensity pressures [37]. Additionally, the band at 878 cm^{-1} relates to S–OH stretching vibrations of H$_2$SO$_4$ in gel matrix [38].

3.2. Ionic conductivity study

Fig. 2(c) represents the discrepancy of ionic conductivity concerning different wt% of ZrO$_2$ in PVA. Plane PVA, 0.5 wt% ZrO$_2$@PVA, 1 wt% ZrO$_2$@PVA, 1.5 wt% ZrO$_2$@PVA and 2 wt% ZrO$_2$@PVA gel systems showed ionic conductivity of 6.45, 6.85, 6.91, 6.89 and 6.87 mS cm^{-1}, respectively. When ZrO$_2$ is mixed to the PVA gel system, an increase in ionic conductivity is observed. Increasing the content of ZrO$_2$ in the PVA substrate from 0.5 to 1 wt% correlates with a rise in ionic conductivity. This is because when ZrO$_2$ is added to PVA, ZrO$_2$ creates defects and free volume in the PVA. These flaws and free volume provide pathways for the ions to move more easily, which increases the ionic conductivity [39]. When the amount of ZrO$_2$ increases from 1 to 2 wt%, a decrease in ionic conductivity is noted. When excess ZrO$_2$ is added beyond 1 wt% to PVA, the ZrO$_2$ can block the pathways for ionic conduction in PVA. This is because the ZrO$_2$ can form oxygen vacancies, which can trap ions and prevent them from moving through PVA. Additionally, the ZrO$_2$ can also form a network of strong hydrogen bonds with the PVA molecules, which can further hinder the movement of ions

Table 1
Impedance parameters of formulated gel systems.

Gel systems	Rs (Ohm)	Cdl (F)	R_1 (Ohm)	Q (S-s^n)	n	Rct (Ohm)	W (S-s^5)
0.5 wt% ZrO_2@PVA	0.5344	0.0002789	2.489	0.005415	0.59	43.05	0.0785
1 wt% ZrO_2@PVA	0.4922	0.0002862	2.296	0.006593	0.62	31.18	0.09283
1.5 wt% ZrO_2@PVA	0.5417	0.0002597	2.649	0.006416	0.57	45.64	0.09132
2 wt% ZrO_2@PVA	0.6681	0.0002412	4.318	0.003434	0.57	71.88	0.09097

through PVA [40]. Therefore, among formulated gel systems 1 wt% ZrO_2@PVA gel electrolyte shows the highest ionic conductivity.

3.3. Water retention study

Fig. 2(d) illustrates a water retention study of 1 wt% ZrO_2@PVA gel system. No obvious volume change was observed when the gel electrolyte was stored for 15 days at room temperature and 59 % humidity signifying that the gel formulation revealed admirable fluid retention. Additionally, the weight retention of the gel electrolyte was assessed by calculating the weight ratio of the gel electrolyte at time t (wt) to its initial weight (w0) under conditions of 25 °C and 59 % humidity [41]. As shown in Fig. 2(d), the gel electrolyte could uphold about 99.73 % of the original weight after 15 days of storing, demonstrating the necessary robustness of the gel electrolyte for long-term use. The PVA and ZrO_2 particles interact with each other through hydrogen bonding. These interactions help to prevent the water molecules from evaporating from the polymer matrix.

3.4. Electrochemical characterizations

Fig. 3(a), (b), (c) and (d) illustrates cyclic voltammograms of 0.5 wt% ZrO_2@PVA, 1 wt% ZrO_2@PVA, 1.5 wt% ZrO_2@PVA and 2 wt % ZrO_2@PVA gel systems, respectively. All CV curves are almost the same suggesting that the electrochemical reaction being studied is reversible. This means that the oxidized and reduced forms of the reactant are in equilibrium with each other and that the reaction can go in either direction with equal ease. Cyclic voltammograms were obtained across a range of scan rates, varying from 10 mV s^{-1} to 150 mV s^{-1}. Distinct anodic and cathodic peaks were observed, indicating the existence of redox reactions within the system. Specifically, an anodic peak appeared at −0.49 V, corresponding to the formation of lead sulfate from lead, while a cathodic peak emerged at −0.64 V, signifying the conversion of lead sulfate back into lead. Additionally, another anodic peak was identified around 0.1 V, attributed to the oxidation of a trace amount of antimony present in the lead electrode. A corresponding cathodic peak at −0.45 V indicated the reduction of lead oxide back to lead [42]. With higher scan rates, the available time for diffusion diminishes, necessitating an increase in current to uphold consistent charge transfer levels.

Fig. 3(e) displays CV curves of all gel systems at a fixed scan rate of 70 mV s^{-1} 0.5 wt% ZrO_2@PVA, 1 wt% ZrO_2@PVA, 1.5 wt% ZrO_2@PVA and 2 wt% ZrO_2@PVA gel systems showed anodic peak current of 0.01036, 0.02351, 0.00999 and 0.00953 A, respectively. From the graph, it is clearly observed that the 1 wt% ZrO_2@PVA gel matrix exhibited the maximum peak current. When ZrO_2 is incorporated into PVA gel, it rises the conductivity of the gel, which leads to an increase in the peak current in the CV curves. Also, ZrO_2 has a high surface area, which means that there are more active sites for electrochemical reactions to occur. This also leads to an increase in the peak current in the CV curves [43]. ZrO_2 particles tend to aggregate when they are in excess. This aggregation can lead to the formation of large particles that are not as electrochemically active as smaller particles [44].

The decreased electrochemical activity of the ZrO_2 particles can also contribute to the decrease in the peak in the CV curve beyond 1 wt% of ZrO_2. The discrepancy of peak current concerning wt% of ZrO_2 at 70 mV s^{-1} is displayed in Fig. 3(f). Fig. 4(a) illustrates the Nyquist plot depicting the impedance characteristics of PVA loaded with various ZrO_2 nano powders, accompanied by the corresponding equivalent circuit. The ZSimpWin 3.21 software facilitated the generation of fitted curves and the choice of appropriate equivalent circuits for analysis. Impedance constraints such as resistance (R), double layer capacitance (Cdl), constant phase element (Q), and Warburg impedance (W) were taken into account to evaluate the impedance properties of the gel. Key impedance parameters including solution resistance (Rs) and charge transfer resistance (Rct) were crucial in assessing the resistance behavior of the gel system. Table 1 presents the impedance analysis results for all gels. Upon examination of Fig. 4(b) and Tables 1 and it becomes evident that the gel system containing 1 wt% ZrO_2@PVA exhibits notably lower values of Rs (0.4922 Ohm) and Rct (31.18 Ohm), alongside higher values of Cdl (0.0002862 F) and Q (0.006593 S-s^n) compared to other ZrO_2-loaded PVA gels. This phenomenon can be ascribed to the heightened presence of mobile ions at this amount, facilitating enhanced electrical conductivity and consequently reducing resistance. Moreover, the 1 wt% ZrO_2@PVA gel system demonstrates a heightened Warburg impedance (0.09283 S-s^5). This observation is indicative of the increased resistance to electron flow introduced by the ZrO_2@PVA composition. Such enhanced resistance contributes to the elevated Warburg impedance observed. These findings collectively underscore the significant impact of ZrO_2@PVA concentration on the electrochemical behavior of the gel system, with implications for its conductivity and performance characteristics.

Fig. 4(c) illustrates galvanostatic charge-discharge curves of optimized 1 wt% ZrO_2@PVA gel system at various current densities. The graph shows that when the current density declines, the time needed to charge and discharge rises. When the current density is high, more charge flows through the system per unit time. This means that the system will charge or discharge more quickly. Conversely, when the current density is low, less charge flows through the system per unit time. This means that the system will charge or discharge more slowly [45]. 1 wt% ZrO_2@PVA gel system took a discharge time of 88, 257, 372 and 1125 s when current density
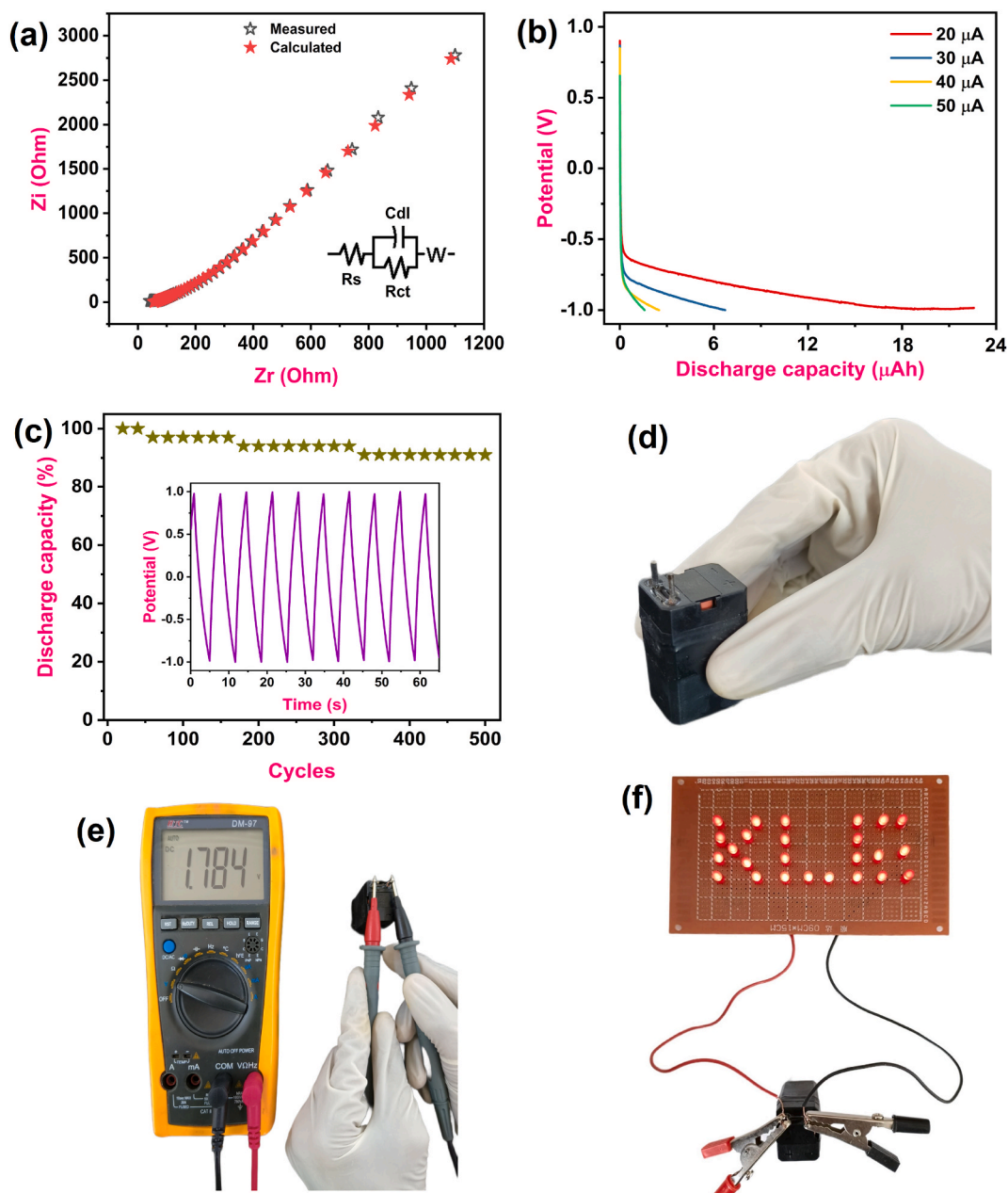
Fig. 5. (a) Nyquist plot of battery device (b) Discharge capacity curves (c) Cycle life of battery device (d–f) photo image of battery device, attained potential of battery device and LED lit with battery device, respectively.

decreased from 1.2, 0.8, 0.7 and 0.6 mA cm^{-2}, respectively. Fig. 4(d) represents discharge capacity findings at different current densities. 1 wt% ZrO$_2$@PVA gel system shows discharge capacity of 30.36, 57.47, 74.43 and 198.45 μAh cm^{-2} at current densities of 1.2, 0.8, 0.7 and 0.6 mA cm^{-2}, respectively. As the current density lowers, the material's discharge capacity increases [46]. When the current density is high, electrolyte ions have less time to move into the material and charge it. This results in a lower discharge capacity. Once the current density is small, the ions have extra time to move into the material and charge it. This results in a higher discharge capacity [47]. 1 wt% ZrO$_2$@PVA gel system maximum discharge capacity of 198.45 μAh cm^{-2} at 0.6 mA cm^{-2} current density.

The battery device is filled with an optimized 1 wt% ZrO$_2$@PVA gel system and subjected to EIS and GCD techniques. Fig. 5(a) displays the fitted Nyquist plot of the battery device. An equivalent circuit model of Rs(CdlRct)W is utilized to fit impedance data. For the battery device Rs, Cdl, Rct and W values are 52.55 Ohm, 8.116 × 10^{-5} F, 1.66 × 10^4 Ohm, 0.0003507 S-s^5, respectively. Furthermore, the discharge capacity of the battery device as a whole was analyzed at different currents and displayed in Fig. 5(b).

Table 2
Comparison study of gel electrolytes.

Gel electrolytes	Peak current	Rs (Ohm)	Rct (Ohm)	References
0.6 wt% S-GrOP	0.09 A	0.216	293.1	[29]
6 wt% FS + 3 wt% TiO_2	0.075 A @ 20 mV s^{-1}	0.42	1.7	[30]
SSCE-FBGE	0.036 A @ 20 mV s^{-1}	1.01	11.82	[48]
6 wt% FS + 0.6 wt% Gibbsite	0.13 A @ 50 mV s^{-1}	0.0475	1720	[49]
6 wt% FS + 0.6 wt% Boehmite	0.10 A @ 50 mV s^{-1}	0.682	563	[49]
20 wt% TEOS@PVA	0.027 A @ 50 mV s^{-1}	0.5182	72.33	[5]
10 wt% PSSAMANa@PVA	0.0236 A @ 50 mV s^{-1}	0.7076	5058	[6]
1 wt% TiO_2@PVA-TEOS	0.014 A @ 50 mV s^{-1}	0.4475	31.12	[38]
3 wt% MnO_2@PVA	0.0485 A @ 100 mV s^{-1}	0.5253	61.44	[10]
4 wt% HNC@PVA	0.086 A @ 100 mV s^{-1}	0.4763	36.22	[50]
8 wt% Graphene@PVA	0.036 A @ 50 mV s^{-1}	0.4684	36.3	[33]
1 wt% ZrO_2@PVA	0.023 A @ 70 mV s^{-1}	0.4922	31.18	This work

Battery devices showed discharge capacities of 1.6, 2.6, 6.7 and 22.5 μAh at the current of 50, 40, 30 and 20 μA, respectively. Battery displayed highest discharge capacity of 22.5 μAh at the current of 20 μA. To analyze the long-term stability of the battery, a cycle study was accomplished for 500 cycles at 50 μA current.

Fig. 5(c) represents the cycle study and battery device along with the nature of the first 10 charge-discharge cycles. After 500 cycles, a remarkable discharge capacity retention of 91 % was found for the battery. Fig. 5(d), (e) and (f) represent photo images of the battery device with 1 wt% ZrO_2@PVA gel system, voltmeter showing 1.784 V for battery, LED lit using our battery device. Table 2 demonstrates the comparison study of gel systems. From the table, one can witness that ZrO_2@PVA gels exhibit better peak current and relatable resistances when compared to the data available in the literature.

4. Conclusions

This work signifies the preparation and characterization of ZrO_2@PVA gel systems for VRLA batteries. Functional groups present in the ZrO_2@PVA gel system are witnessed by FTIR techniques. 1 wt% ZrO_2@PVA gel system showed the maximum ionic conductivity of 6.91 mS cm^{-1} and water retention of 99.73 % for up to 15 days. From CV curves, 1 wt% ZrO_2@PVA gel system showed the highest anodic peak of 0.02351 A. From EIS data, 1 wt% ZrO_2@PVA gel system exhibited the lowest Rs (0.4922 Ohm) and Rct (31.18 Ohm) values. GCD suggested that 1 wt% ZrO_2@PVA gel system exhibited a discharge capacity of 198.45 μAh cm^{-2} at 0.6 mA cm^{-2} current density. Battery device with optimized 1 wt% ZrO_2@PVA gel system displayed a maximum discharge capacity of 22.5 μAh at the current of 20 μA. After 500 continuous cycles, battery attained a discharge capacity retention of 91 %. Current electrochemical data suggest that ZrO_2 can be used as an additive for PVA gel electrolytes in VRLA battery applications.

Data availability

Data will be made available on request.

CRediT authorship contribution statement

Sanjay H. Rajur: Writing – original draft, Methodology, Conceptualization. **Bipin S. Chikkatti:** Writing – original draft, Investigation. **Abdulwasa Bakr Barnawi:** Writing – review & editing, Formal analysis, Conceptualization. **Javed Khan Bhutto:** Writing – review & editing. **T.M. Yunus Khan:** Writing – review & editing, Funding acquisition. **Ashok M. Sajjan:** Writing – review & editing, Supervision, Conceptualization. **Nagaraj R. Banapurmath:** Writing – review & editing, Project administration, Formal analysis. **A.B. Raju:** Writing – review & editing.

Declaration of competing interest

The authors declare that they have no known competing financial interests or personal relationships that could have appeared to influence the work reported in this paper.

References

[1] A. Ahmad, A. Khan, N. Javaid, H.M. Hussain, W. Abdul, A. Almogren, A. Alamri, I.A. Niaz, An optimized home energy management system with integrated renewable energy and storage resources, Energies 10 (2017), https://doi.org/10.3390/en10040549.

[2] A.R. Dehghani-Sanij, E. Tharumalingam, M.B. Dusseault, R. Fraser, Study of energy storage systems and environmental challenges of batteries, Renew. Sustain. Energy Rev. 104 (2019) 192–208, https://doi.org/10.1016/j.rser.2019.01.023.

[3] V. Palomares, P. Serras, I. Villaluenga, K.B. Hueso, J. Carretero-González, T. Rojo, Na-ion batteries, recent advances and present challenges to become low cost energy storage systems, Energy Environ. Sci. 5 (2012) 5884–5901, https://doi.org/10.1039/c2ee02781j.

[4] G.J. May, A. Davidson, B. Monahov, Lead batteries for utility energy storage: a review, J. Energy Storage 15 (2018) 145–157, https://doi.org/10.1016/j.est.2017.11.008.

[5] B.S. Chikkatti, A.M. Sajjan, P.B. Kalahal, N.R. Banapurmath, T.M.Y. Khan, S.D.A. Khadar, S.M. Shamsudeen, A.B. Raju, A novel poly(vinyl alcohol)–tetraethylorthosilicate hybrid gel electrolyte for lead storage battery, Gels 8 (12) (2022) 791, https://doi.org/10.3390/gels8120791.

[6] B.S. Chikkatti, A.M. Sajjan, P.B. Kalahal, N.R. Banapurmath, Insight into the performance of valve-regulated lead-acid battery using sodium salt of poly(4-styrene sulfonic acid-co-maleic acid)-poly(vinyl alcohol) gel electrolyte, J. Energy Storage 72 (2023) 108261, https://doi.org/10.1016/j.est.2023.108261.

[7] W.L. Chou, Removal and adsorption characteristics of polyvinyl alcohol from aqueous solutions using electrocoagulation, J. Hazard Mater. 177 (2010) 842–850, https://doi.org/10.1016/j.jhazmat.2009.12.110.

[8] R. Surudžić, A. Janković, N. Bibić, M. Vukašinović-Sekulić, A. Perić-Grujić, V. Mišković-Stanković, S.J. Park, K.Y. Rhee, Physico-chemical and mechanical properties and antibacterial activity of silver/poly(vinyl alcohol)/graphene nanocomposites obtained by electrochemical method, Compos. B Eng. 85 (2016) 102–112, https://doi.org/10.1016/j.compositesb.2015.09.029.

[9] D. Coviello, M. Contursi, R. Toniolo, I.G. Casella, Electrochemical and spectroscopic investigation of a binary Ni-Co oxide active material deposited on graphene/polyvinyl alcohol composite substrate, J. Electroanal. Chem. 791 (2017) 117–123, https://doi.org/10.1016/j.jelechem.2017.02.048.

[10] B.S. Chikkatti, A.M. Sajjan, N.R. Banapurmath, The state of understanding of the electrochemical behaviours of a valve-regulated lead–acid battery comprising manganese dioxide-impregnated gel polymer electrolyte, Mater. Adv. 4 (23) (2023) 6192–6198, https://doi.org/10.1039/D3MA00563A.

[11] A.R. Polu, R. Kumar, Preparation and characterization of pva based solid polymer electrolytes for electrochemical cell applications, Chin. J. Polym. Sci. 31 (2013) 641–648, https://doi.org/10.1007/s10118-013-1246-3.

[12] Z. Cui, Z. Zheng, L. Lin, J. Si, Q. Wang, X. Peng, W. Chen, Electrospinning and crosslinking of polyvinyl alcohol/chitosan composite nanofiber for transdermal drug delivery, Adv. Polym. Technol. 37 (2018) 1917–1928, https://doi.org/10.1002/adv.21850.

[13] G. Merle, S.S. Hosseiny, M. Wessling, K. Nijmeijer, New cross-linked PVA based polymer electrolyte membranes for alkaline fuel cells, J Memb Sci 409–410 (2012) 191–199, https://doi.org/10.1016/j.memsci.2012.03.056.

[14] M. Penza, G. Cassano, Relative humidity sensing by PVA-coated dual resonator SAW oscillator, Sens. Actuators B: Chem. 68 (1–3) (2000) 300–306, https://doi.org/10.1016/S0925-4005(00)00448-2.

[15] L. Fan, H. Yang, J. Yang, M. Peng, J. Hu, Preparation and characterization of chitosan/gelatin/PVA hydrogel for wound dressings, Carbohydr. Polym. 146 (2016) 427–434, https://doi.org/10.1016/j.carbpol.2016.03.002.

[16] B.S. Chikkatti, A.M. Sajjan, P.B. Kalahal, N.R. Banapurmath, N.H. Ayachit, Fabrication and assessment of poly(lactic acid) - poly(4-styrene sulfonate) flexible membranes as electrodes for supercapacitors, J. Energy Storage 72 (2023) 108513, https://doi.org/10.1016/j.est.2023.108513.

[17] K. Palanichamy, M. Anandan, J. Sridhar, V. Natarajan, A. Dhandapani, PVA and PMMA nano-composites: a review on strategies, applications and future prospects, Mater. Res. Express 10 (2023), https://doi.org/10.1088/2053-1591/acb527.

[18] Y.S. Zhu, X.J. Wang, Y.Y. Hou, X.W. Gao, L.L. Liu, Y.P. Wu, M. Shimizu, A new single-ion polymer electrolyte based on polyvinyl alcohol for lithium ion batteries, Electrochim. Acta 87 (2013) 113–118, https://doi.org/10.1016/j.electacta.2012.08.114.

[19] A.K. Solarajan, V. Murugadoss, S. Angaiah, Dimensional stability and electrochemical behaviour of ZrO₂ incorporated electrospun PVdF-HFP based nanocomposite polymer membrane electrolyte for Li-ion capacitors, Sci. Rep. 7 (1) (2017) 45390, https://doi.org/10.1038/srep45390.

[20] N.Y. Mostafa, M.M. Qhtani, S.H. Alotaibi, Z.I. Zaki, S. Alharthi, M. Cieslik, K. Gornicka, J. Ryl, R. Boukherroub, M.A. Amin, Cathodic activation of synthesized highly defective monoclinic hydroxyl-functionalized ZrO₂ nanoparticles for efficient electrochemical production of hydrogen in alkaline media, Int. J. Energy Res. 44 (2020) 10695–10709, https://doi.org/10.1002/er.5713.

[21] S. Huo, H. Zhao, J. Dong, J. Xu, Facile synthesis of ordered mesoporous zirconia for electrochemical enrichment and detection of organophosphorus pesticides, Electroanalysis 30 (2018) 2121–2130, https://doi.org/10.1002/elan.201800284.

[22] C.C. Yang, Study of alkaline nanocomposite polymer electrolytes based on PVA-ZrO2-KOH, Mater Sci Eng B Solid State Mater Adv Technol 131 (2006) 256–262, https://doi.org/10.1016/j.mseb.2006.04.036.

[23] Y. Jiang, G. Cheng, Y. Li, Z. He, J. Zhu, W. Meng, L. Dai, L. Wang, Promoting vanadium redox flow battery performance by ultra-uniform ZrO₂@C from metal-organic framework, Chem. Eng. J. 415 (2021) 129014, https://doi.org/10.1016/j.cej.2021.129014.

[24] S.E. Naleway, K.C. Fickas, Y.N. Maker, M.A. Meyers, J. McKittrick, Reproducibility of ZrO₂-based freeze casting for biomaterials, Mater. Sci. Eng. C 61 (2016) 105–112, https://doi.org/10.1016/j.msec.2015.12.012.

[25] R. Zhang, X. Zhang, S. Hu, High temperature and pressure chemical sensors based on Zr/ZrO₂ electrode prepared by nanostructured ZrO₂ film at Zr wire, Sens Actuators B Chem 149 (2010) 143–154, https://doi.org/10.1016/j.snb.2010.06.009.

[26] X. Li, Y. Yu, Y. Meng, Novel quaternized poly(arylene ether sulfone)/nano-ZrO2 composite anion exchange membranes for alkaline fuel cells, ACS Appl. Mater. Interfaces 5 (2013) 1414–1422, https://doi.org/10.1021/am302844x.

[27] P.J. Lee, C.C. Ho, C.S. Hwang, S.J. Ding, Improved physicochemical properties and biocompatibility of stainless steel implants by PVA/ZrO2-based composite coatings, Surf. Coat. Technol. 258 (2014) 374–380, https://doi.org/10.1016/j.surfcoat.2014.08.066.

[28] W. Xiao, J. Song, L. Huang, Z. Yang, Q. Qiao, PVA-ZrO2 multilayer composite separator with enhanced electrolyte property and mechanical strength for lithium-ion batteries, Ceram. Int. 46 (2020) 29212–29221, https://doi.org/10.1016/j.ceramint.2020.08.095.

[29] A. Mansuroglu, M. Gencten, M.B. Arvas, M. Sahin, A.E. Bozdogan, Y. Sahin, A novel electrolyte additive for gel type valve regulated lead acid batteries: sulfur doped graphene oxide, Int. J. Energy Res. 45 (2021) 21390–21402, https://doi.org/10.1002/er.7189.

[30] Y. Sahin, M. Gencten, K.B. Donmez, A novel gel electrolyte for valve-regulated lead acid battery, Anadolu University J. Sci. Technol A - Appl. Sci. Eng. 18 (2017), https://doi.org/10.18038/aubtda.300420, 146–146.

[31] G.K. Sidhu, A.K. Kaushik, S. Rana, S. Bhansali, R. Kumar, Photoluminescence quenching of Zirconia nanoparticle by surface modification, Appl. Surf. Sci. 334 (2015) 216–221, https://doi.org/10.1016/j.apsusc.2014.10.036.

[32] R.S. Das, S.K. Warkhade, A. Kumar, A.V. Wankhade, Graphene oxide-based zirconium oxide nanocomposite for enhanced visible light-driven photocatalytic activity, Res. Chem. Intermed. 45 (2019) 1689–1705, https://doi.org/10.1007/s11164-018-3699-z.

[33] M.M. Gomaa, C. Hugenschmidt, M. Dickmann, E.E. Abdel-Hady, H.F.M. Mohamed, M.O. Abdel-Hamed, Crosslinked PVA/SSA proton exchange membranes: correlation between physiochemical properties and free volume determined by positron annihilation spectroscopy, Phys. Chem. Chem. Phys. 20 (2018) 28287–28299, https://doi.org/10.1039/c8cp05301d.

[34] H. Awada, C. Daneault, Chemical modification of poly(vinyl alcohol) in water, Appl. Sci. 5 (2015) 840–850, https://doi.org/10.3390/app5040840.

[35] B.S. Chikkatti, A.M. Sajjan, N.H. Ayachit, Graphene-Doped hydrogels promoting ionic conductivity in gel-valve-regulated lead acid batteries, Langmuir 39 (48) (2023) 17232–17239, https://doi.org/10.1021/acs.langmuir.3c02285.

[36] J. Lee, T. Isobe, M. Senna, Magnetic properties of ultrafine magnetite particles and their slurries prepared via in-situ precipitation, Colloids Surf. A: Physicochem. Eng. Asp. 109 (1996) 121–127, https://doi.org/10.1016/0927-7757(95)03479-X.

[37] R.C. de A.G. Mota, E.O. da Silva, L.R. de Menezes, Effect of the addiction of metal oxide nanoparticles on the physical, chemical and thermal properties of PVA based nanocomposites, Mater. Sci. Appl. 9 (2018) 473–488.

[38] B.S. Chikkatti, A.M. Sajjan, P.B. Kalahal, N.R. Banapurmath, A.R. Angadi, Insight into the performance of VRLA battery using PVA-TEOS hybrid gel electrolytes with titania nanoparticles, J. Energy Storage 72 (2023) 108572, https://doi.org/10.1016/j.est.2023.108572.

[39] V.G. Zavodinsky, The mechanism of ionic conductivity in stabilized cubic zirconia, Phys. Solid State 46 (2004) 453–457, https://doi.org/10.1134/1.1687859.

[40] S. Ladjouzi, L. Guerbous, Structural and optical properties of PVA/ZrO$_2$:Eu^{3+} hybrid films prepared via γ-irradiation, n.d. ,. doi:10.2139/ssrn.4540873.

[41] C. Jiang, T. Zhu, H. Liu, G. Yang, Z. He, M. Wang, M. Ji, G. Cong, J. Yu, C. Zhu, J. Xu, A one-step aqueous route to prepare polyacrylonitrile-based hydrogels with excellent ionic conductivity and extreme low temperature tolerance, J Mater Chem A Mater 8 (2020) 22090–22099, https://doi.org/10.1039/d0ta08177a.

[42] W. Visscher, Cyclic voltammetry on lead electrodes in sulphuric acid solution, J. Power Sources 1 (3) (1976) 257–266, https://doi.org/10.1016/0378-7753(76)81003-8.

[43] C.H. Comninellis, G.P. Vercesi, Characterization of DSA®-type oxygen evolving electrodes: choice of a coating, J. Appl. Electrochem. 21 (1991) 335–345, https://doi.org/10.1007/BF01020219.

[44] S. Shukla, S. Seal, Mechanisms of room temperature metastable tetragonal phase stabilisation in zirconia, Int. Mater. Rev. 50 (2005) 45–64, https://doi.org/10.1179/174328005X14267.

[45] H.B. Huntington, A.R. Crone, Current-induced marker motion in gold wires, J. Phys. Chem. Solids 20 (1–2) (1961) 76–87, https://doi.org/10.1016/0022-3697(61)90138-X.

[46] Chikkatti B.S., Sajjan A.M., Banapurmath N.R., Bhutto J.K., Verma R., Yunus Khan T.M., Fabrication of flexible films for supercapacitors using halloysite nanoclay incorporated poly (lactic acid), Polymers 15 (23) (2023) 4587, doi:10.3390/polym15234587.

[47] Y. Sun, X. Hu, W. Luo, F. Xia, Y. Huang, Reconstruction of conformal nanoscale MnO on graphene as a high-capacity and long-life anode material for lithium ion batteries, Adv. Funct. Mater. 23 (2013) 2436–2444, https://doi.org/10.1002/adfm.201202623.

[48] K.B. Dönmez, M. Gençten, Y. Şahin, A performance comparison of protective silicate-coated lead and non-coated lead electrodes in various kind electrolytes of gel valve-regulated lead-acid battery, Ionics 24 (2018) 3655–3664, https://doi.org/10.1007/s11581-018-2551-1.

[49] M. Gençten, Investigation the effects of boehmite and gibbsite on the electrochemical behaviours of Gel-VRLA batteries, Int. J. Electrochem. Sci. 13 (2018) 11741–11751, https://doi.org/10.20964/2018.12.15.

[50] B.S. Chikkatti, A.M. Sajjan, N.R. Banapurmath, Facilitating ionic conduction in the valve-regulated lead acid battery by poly(vinyl alcohol)-halloysite nano-clay gel polymer electrolyte, Energy Technol. (2024) 2301265, https://doi.org/10.1002/ente.202301265.